

# Experimental and Theoretical Approaches to Redox Innocence of Ligands in Uranyl Complexes: What Is Formal Oxidation State of Uranium in Reductant of Uranyl(VI)?

Koichiro Takao,<sup>\*,†</sup> Satoru Tsushima,<sup>‡</sup> Toshinari Ogura,<sup>†</sup> Taro Tsubomura,<sup>§</sup> and Yasuhisa Ikeda<sup>†</sup>

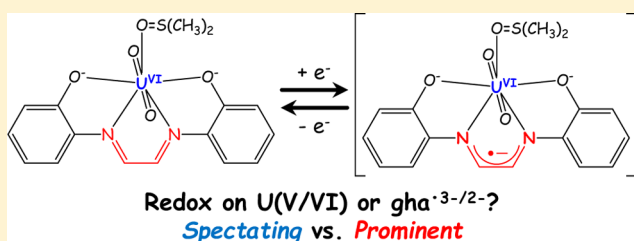
<sup>†</sup>Research Laboratory for Nuclear Reactors, Tokyo Institute of Technology, 2-12-1 Ōokayama, Meguro-ku, 152-8550 Tokyo, Japan

<sup>‡</sup>Institute of Resource Ecology, Helmholtz-Zentrum Dresden-Rossendorf, P.O. Box 51 01 19, 01314 Dresden, Germany

<sup>§</sup>Department of Materials and Life Science, Seikei University, 3-3-1 Kichijoji-kitamachi, Musashino-shi, 180-8633 Tokyo, Japan

## Supporting Information

**ABSTRACT:** Redox behavior of  $[\text{UO}_2(\text{gha})\text{DMSO}]^- / \text{UO}_2(\text{gha})\text{DMSO}$  couple (gha = glyoxal bis(2-hydroxanil)ate, DMSO = dimethyl sulfoxide) in DMSO solution was investigated by cyclic voltammetry and UV-vis-NIR spectroelectrochemical technique, as well as density functional theory (DFT) calculations.  $[\text{UO}_2(\text{gha})\text{DMSO}]^-$  was found to be formed via one-electron reduction of  $\text{UO}_2(\text{gha})\text{DMSO}$  without any successive reactions. The observed absorption spectrum of  $[\text{UO}_2(\text{gha})\text{DMSO}]^-$ , however, has clearly different characteristics from those of uranyl(V) complexes reported so far. Detailed analysis of molecular orbitals and spin density of the redox couple showed that the  $\text{gha}^{2-}$  ligand in  $\text{UO}_2(\text{gha})\text{DMSO}$  is reduced to  $\text{gha}^{3-}$  to give  $[\text{UO}_2(\text{gha})\text{DMSO}]^-$  and the formal oxidation state of U remains unchanged from +6. In contrast, the additional DFT calculations confirmed that the redox reaction certainly occurs at the U center in other uranyl(V/VI) redox couples we found previously. The *noninnocence* of the Schiff base ligand in the  $[\text{UO}_2(\text{gha})\text{DMSO}]^- / \text{UO}_2(\text{gha})\text{DMSO}$  redox couple is due to the lower energy level of LUMO in this ligand relative to those of U 5f orbitals. This is the first example of the *noninnocent* ligand system in the coordination chemistry of uranyl(VI).



## 1. INTRODUCTION

It is well-known that uranium, neptunium, and plutonium in the early actinide series show rich redox chemistry in contrast to the lanthanide elements. Their oxidation state may vary from III to VI (or even II and VII under some specific conditions).<sup>1</sup> The variety of the oxidation numbers facilitates mutual separation of these actinide elements, and their recovery from a mixture with other elements like fission products.<sup>2</sup> This is the most fundamental and important basis of reprocessing methods for spent nuclear fuels. The rich redox chemistry of these actinides and related coordination behavior are also highly relevant for understanding of their environmental mobility in geological disposal of radioactive wastes.<sup>3</sup>

At V and VI oxidation states, U, Np, and Pu generally form actinyl ions,  $[\text{MO}_2]^{n+}$  ( $n = 1, 2$ ), in solutions.<sup>1</sup> These species exhibit unique coordination behavior arising from their linear  $[\text{O}=\text{M}=\text{O}]^{2+}$  geometries, that is, additional ligands can interact with the metal centers only in the equatorial planes of the actinyl ions. The uranyl(V) is usually very unstable because of its sensitivity toward oxidation and disproportionation.<sup>1,4</sup> Therefore, its chemistry had been rather exotic and not well understood previously. After the unexpected isolation of tetrakis(triphenylphosphine oxide)dioxouranium(V) triflate by Berthet et al.<sup>5</sup> and our finding of a uranyl(V) complex stabilized by an auxiliary tetradentate Schiff base ligand

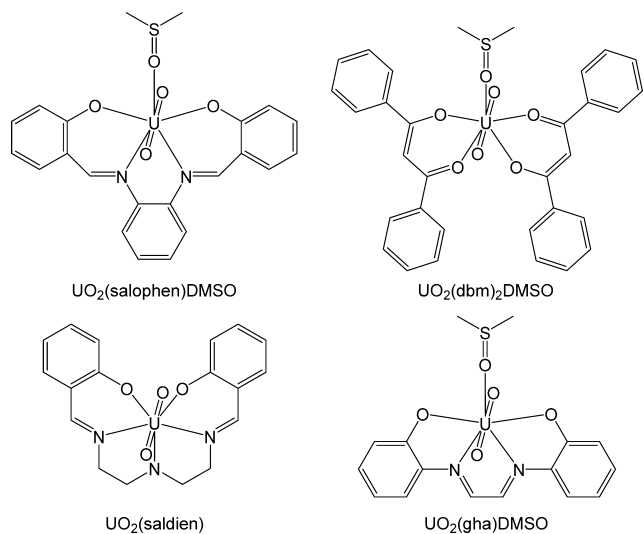
( $[\text{U}^{\text{V}}\text{O}_2(\text{salophen})\text{DMSO}]^-$ , Chart 1),<sup>6</sup> the coordination chemistry of uranyl(V) has been explored in the past decade.<sup>7–11</sup> As a result, various aspects including photophysical properties, molecular structures, and reactivity of uranyl(V) complexes were clarified. Most works started from uranyl(VI) compounds as parent species to prepare uranyl(V) through electrochemical or chemical one-electron reduction. All the former works thought that ligands surrounding U are redox-inactive or *innocent* as designated by C. K. Jørgensen.<sup>12</sup> This could be reasonable in a traditional sense, because the nonbonding  $5f\delta_u$  and  $5f\phi_u$  orbitals are lying at the lowest energy among vacant orbitals,<sup>13</sup> and therefore the electron injected into a uranyl(VI) species should be placed to one of them. In contrast, unoccupied molecular orbitals arising from ligands should have antibonding character, which gives them higher energy than the nonbonding ones like  $5f\delta_u$  and  $5f\phi_u$ . Therefore, ligands just play a spectator role in the redox reactions.

Recently, it was clarified for various transition metal complexes of which ligands are not always *innocent* toward the redox reaction, but are sometimes also redox-active, namely, *noninnocent*. The latest findings and its attractive aspects in

Received: March 19, 2014

Published: May 21, 2014

Chart 1. Schematic Structures of Uranyl(VI) Complexes



catalytic chemistry are summarized in a Forum of *Inorganic Chemistry*<sup>14</sup> and several comprehensive reviews.<sup>15</sup> In this manner, metal and ligand(s) can synergistically cooperate, and ligands can also play a much more prominent role in the elementary bond activation steps in a catalytic cycle. The *noninnocence* of ligands would be found also in the coordination chemistry of the actinides. However, such an issue has not been dealt with in detail so far, while there are only a few discussions on low-valent organoactinides<sup>16</sup> as well as on octavalent plutonium.<sup>17</sup> This situation should arise from the fact that experimental evidence indicating the *noninnocent* behavior of ligands in an actinide complex has been poorly obtained.

In this article, we present the first example of a redox *noninnocent* ligand, glyoxal bis(2-hydroxanilate) ( $\text{gha}^{2-}$ ), in its uranyl complex,  $\text{UO}_2(\text{gha})\text{DMSO}$  (Chart 1). This chemistry was studied by both experimental and theoretical approaches using electro- and spectroelectrochemical techniques and quantum chemical (DFT) calculations. Other uranyl(V/VI) redox couples we found formerly (Chart 1)<sup>6,7</sup> were also investigated by the same computational method to confirm that (1) their ligands are really redox *innocent* and (2) the formal oxidation states of U in the reductants are really +5.

## 2. EXPERIMENTAL AND COMPUTATIONAL DETAILS

**2.1. Materials.** Pentakis(dimethyl sulfoxide)dioxouranium(VI) perchlorate,  $[\text{UO}_2(\text{DMSO})_5](\text{ClO}_4)_2$ , was prepared by replacing *N,N*-dimethylacetamide (DMA) with dimethyl sulfoxide (DMSO) in a procedure to obtain the similar DMA solvate reported by Bowen et al.<sup>18</sup> The DMSO solvent (Kanto Chemical Co., Ind.) used in the electro- and spectroelectrochemical experiments was dried over 4A molecular sieves (Wako). Tetra-*n*-butylammonium hexafluorophosphate (TBAPF<sub>6</sub>, Wako) was used without further purification. All other chemicals were of reagent grade and used as received.

**2.2. Preparation of  $\text{UO}_2(\text{gha})\text{DMSO}$ .**<sup>19</sup> Opaque white powder of glyoxal bis(2-hydroxanilate) ( $\text{H}_2\text{gha}$ ) was prepared by condensation between *o*-aminophenol (0.781 g) and glyoxal (40 wt % aqueous 0.513 g) in degassed and warmed ethanol (9 mL) under argon atmosphere, followed by filtration, washing with *n*-pentane, and drying under suction. Yield: 0.625 g (74%). <sup>1</sup>H NMR (400 MHz,  $\text{CDCl}_3$ ,  $\delta$ /ppm vs TMS): 6.90–6.65 (m, 8H, Ph–H), 5.33 (s, 2H, N=CH), 4.89 (bs, 2H, OH).

In a Schlenk flask filled with argon,  $\text{H}_2\text{gha}$  (0.045 g) was dissolved in methanol (5 mL) degassed by purging dry argon gas for 10 min prior to use. Three droplets of pyridine were also loaded in this

reaction mixture. To this solution was added dropwise  $\text{UO}_2(\text{DMSO})_5(\text{ClO}_4)_2$  (0.158 g) dissolved in hot methanol (2 mL), followed by vigorous stirring for 3 h at room temperature in the dark. The supernatant was removed by syringe through a septum cap, and the residue was washed with the degassed methanol (3 × 3 mL). The deep purple residue in the flask was dried under suction at room temperature. Yield: 0.070 g (68%). Characterization has been performed by using <sup>1</sup>H NMR and IR spectroscopy. <sup>1</sup>H NMR (400 MHz,  $\text{DMSO}-d_6$ ,  $\delta$ /ppm vs TMS): 9.45 (s, 2H, –N=CH–), 7.95 (dd, 2H, Ph–H), 7.51 (td, 2H, Ph–H), 6.9–6.8 (m, 4H, Ph–H), 2.58 (s, 6H, O=S(CH<sub>3</sub>)<sub>2</sub>). IR (KBr pellet,  $\nu/\text{cm}^{-1}$ ): 950 (O=U=O asymmetric stretching), 995 (S=O stretching), 1584 (C=N stretching).

**2.3. Methods.** Cyclic voltammetry (CV) measurements were performed at 298 K under a dry argon atmosphere using BAS ALS660B. A three-electrode system consisted of a Pt disk working electrode (electrode surface area: 0.020 cm<sup>2</sup>), a Pt wire counter electrode, and an Ag/Ag<sup>+</sup> reference electrode (BAS RE-5B, 0.1 M TBAClO<sub>4</sub> + 0.01 M AgNO<sub>3</sub>/CH<sub>3</sub>CN). A ferrocene/ferrocenium ion redox couple (Fc/Fc<sup>+</sup>) was taken as the internal reference redox system.<sup>20</sup> Dissolved oxygen gas in the sample solutions was removed by passing argon gas through for at least 20 min prior to starting experiments. To compensate the *iR* drops, the cyclic voltammograms of the blank solution (0.1 M TBAPF<sub>6</sub>/DMSO) were also recorded under the same potential sweep rate and potential range, and subtracted from those of  $\text{UO}_2(\text{gha})\text{DMSO}$  in DMSO.

UV–vis spectroelectrochemical measurements for  $\text{UO}_2(\text{gha})\text{DMSO}$  in DMSO were performed with a SHIMADZU UV-3150 spectrophotometer equipped with an optically transparent thin layer electrode (OTTLE) cell.<sup>21</sup> Its optical path length was  $2.1 \times 10^{-2}$  cm. The three-electrode system was the same as that in the CV experiment with a replacement of the working electrode by a Pt gauze (80 mesh). The potential on OTTLE was controlled by BAS ALS660B. The absorption spectrum at each potential was recorded after equilibrium of the electrochemical reaction, which completed within 2 min. The sample solution in the OTTLE cell was deoxygenated by passing dry argon gas through at least 20 min prior to starting the experiment.

From a  $\text{CH}_2\text{Cl}_2$ /ethanol solution dissolving  $\text{UO}_2(\text{gha})\text{DMSO}$ , purple-black crystals of a desolvated dinuclear species,  $[\text{UO}_2(\text{gha})]_2$ , deposited. A single crystal X-ray diffraction experiment for this compound was performed using the following procedure. The single crystal was mounted in a cryo-loop together with paraffin oil and placed in a low-temperature nitrogen gas stream at 213 K. Intensity data were collected using an imaging plate area detector in a Rigaku RAXIS RAPID diffractometer with graphite-monochromated Mo  $K\alpha$  radiation ( $\lambda = 0.71075 \text{ \AA}$ ). The structure of  $[\text{UO}_2(\text{gha})]_2$  was solved by the SIR92 direct method<sup>22</sup> and expanded using Fourier techniques. All non-hydrogen atoms were anisotropically refined using SHELXL-97.<sup>23</sup> Each hydrogen atom included in the structure was refined as riding on its parent carbon atom with  $U_{\text{iso}}(\text{H}) = 1.2U_{\text{eq}}(\text{C})$ . The final cycle of full-matrix least-squares refinement on  $F^2$  was based on observed reflections and parameters, and converged with unweighted and weighted agreement factors, *R* and *wR*. All computations were performed using the CrystalStructure crystallographic software package.<sup>24</sup> Crystallographic data for  $[\text{UO}_2(\text{gha})]_2$ :  $\text{C}_{28}\text{H}_{20}\text{N}_4\text{O}_8\text{U}$ ;  $M_w = 1016.55$ ;  $0.456 \times 0.432 \times 0.400 \text{ mm}^3$ ; orthorhombic; *Pbca* (61);  $a = 14.4373(5)$ ,  $b = 12.5919(4)$ ,  $c = 14.7778(5) \text{ \AA}$ ;  $V = 2686.5(2) \text{ \AA}^3$ ;  $Z = 4$ ;  $\rho_{\text{calcd}} = 2.513 \text{ Mg}\cdot\text{m}^{-3}$ ;  $\mu = 12.105 \text{ mm}^{-1}$ ;  $T = 213 \text{ K}$ ; 24726 reflections; 3070 independent;  $R_{\text{int}} = 0.0824$ ;  $R = 0.0338$  ( $[F^2 > 2\sigma(F^2)]$ );  $wR = 0.0723$  (all data); GOF = 1.068;  $\Theta = 3.10$  to  $27.47^\circ$ ;  $\Delta\rho_{\text{max}} = 1.530 \text{ e}^- \cdot \text{\AA}^{-3}$ ;  $\Delta\rho_{\text{min}} = -1.630 \text{ e}^- \cdot \text{\AA}^{-3}$ . The ORTEP drawing is shown in Figure S1 in the Supporting Information.

**2.4. DFT Calculations.**  $[\text{UO}_2(\text{gha})\text{DMSO}]^-/\text{UO}_2(\text{gha})\text{DMSO}$ ,  $[\text{UO}_2(\text{salophen})\text{DMSO}]^-/\text{UO}_2(\text{salophen})\text{DMSO}$ ,  $[\text{UO}_2(\text{dbm})_2\text{DMSO}]^-/\text{UO}_2(\text{dbm})_2\text{DMSO}$ , and  $[\text{UO}_2(\text{saldien})]^-/\text{UO}_2(\text{saldien})$  were tested. All calculations were performed using the Gaussian 09 (Rev. C.01) program<sup>25</sup> employing the DFT method with Becke's three-parameter hybrid functional and Lee–Yang–Parr's gradient-corrected correlation functional (B3LYP).<sup>26</sup> For uranium, the effective core potential and basis set were provided by Stuttgart

RSC ECP.<sup>27</sup> The most diffuse basis functions on uranium with the exponent 0.005 (all s, p, d, and f type functions) were omitted as in previous studies.<sup>28</sup> The 6-31G(d,p) basis sets were used for other elements (C, H, N, O, S). Atomic coordinates of each complex were obtained from the reported crystal structure of the same or a similar compound<sup>17b,29</sup> and optimized to be energy minima through vibrational frequency analysis where no imaginary frequency was found to be present. Twenty singlet excited states of  $\text{UO}_2(\text{gha})\text{DMSO}$  were included in the time-dependent (TD) DFT calculations. Spin-orbit effect and the basis set superposition error corrections were neglected.

### 3. RESULTS AND DISCUSSION

**3.1. Characterization and Electro- and Spectroelectrochemistry of  $\text{UO}_2(\text{gha})\text{DMSO}$ .** The parent uranyl(VI) complex,  $\text{UO}_2(\text{gha})\text{DMSO}$ , was obtained from a reaction between  $\text{H}_2\text{gha}$  and  $\text{UO}_2(\text{DMSO})_5(\text{ClO}_4)_2$  in the degassed methanol with moderate yield. Although this compound has already been reported by Cattalini et al.,<sup>19</sup> it is worthwhile to present some comments concerning its coordination chemistry. The structure determination of the single crystal deposited from the  $\text{CH}_2\text{Cl}_2/\text{ethanol}$  solution revealed that a dimeric complex,  $[\text{UO}_2(\text{gha})]_2$ , was formed. A similar dimerization in the chlorinated noncoordinating solvents has also been observed in other uranyl(VI) complexes with the tetradentate Schiff base ligand, salophen<sup>2-29b</sup>. The  $^1\text{H}$  NMR spectrum of a  $\text{DMSO}-d_6$  solution dissolving the product indicated the  $C_{2v}$  symmetry of the  $\text{UO}_2(\text{gha})$  moiety. Furthermore, the NMR signal at 2.58 ppm arises from free  $\text{DMSO}$  which has been involved in the solid compound. This solvent molecule seems to be replaced by  $\text{DMSO}-d_6$  and released to the bulk.<sup>30</sup> The peak integral clearly demonstrates that the stoichiometry of  $\text{DMSO}$  to  $\text{UO}_2(\text{gha})$  is 1:1. Additionally, the IR spectrum of the solid compound shows the characteristic peaks of  $\text{O}=\text{U}=\text{O}$  asymmetric stretching ( $\nu_3$ ,  $950\text{ cm}^{-1}$ ),  $\text{S}=\text{O}$  stretching ( $995\text{ cm}^{-1}$ ), and  $\text{C}=\text{N}$  stretching ( $1584\text{ cm}^{-1}$ ). The  $\nu_3$  frequency disagrees with  $890\text{ cm}^{-1}$  reported by Cattalini et al.<sup>19</sup> Our assignment should be more reliable, because it is supported by the DFT calculation discussed later.

Cyclic voltammograms of  $\text{UO}_2(\text{gha})\text{DMSO}$  ( $3.24 \times 10^{-3}\text{ mol}\cdot\text{dm}^{-3} = M$ ) in  $\text{DMSO}$  containing  $0.1\text{ M}$   $\text{TBAPF}_6$  are shown in Figure 1. The electrochemical data from this figure are listed in Table S1 (Supporting Information). Cathodic and anodic peaks were observed at  $-1.23\text{ V}$  ( $E_{\text{pc}}$ ) and  $-1.16\text{ V}$  ( $E_{\text{pa}}$ )

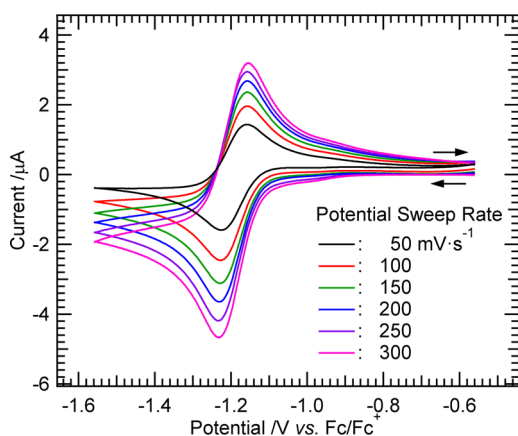


**Figure 1.** Cyclic voltammograms of  $\text{UO}_2(\text{gha})\text{DMSO}$  ( $3.24 \times 10^{-3}\text{ M}$ ) in  $\text{DMSO}$  containing  $0.1\text{ M}$   $\text{TBAPF}_6$ . Initial scan direction: cathodic.

vs  $\text{Fc}/\text{Fc}^+$ , respectively. In each run, the formal potential ( $E^{\circ'} = (E_{\text{pc}} + E_{\text{pa}})/2$ ) is constant at  $-1.194\text{ V}$  vs  $\text{Fc}/\text{Fc}^+$  within  $1\text{ mV}$  error regardless of different potential sweep rate ( $\nu$ ), implying that the reduction and oxidation observed here are coupled with each other. The peak potential separation ( $\Delta E_p = |E_{\text{pc}} - E_{\text{pa}}|$ ) is almost constant at  $0.070\text{ V}$  at  $\nu = 0.050$  to  $0.150\text{ V}\cdot\text{s}^{-1}$ , while it slightly increases at the faster  $\nu$ . This shows shift of the redox reaction from an electrochemically reversible system to the quasireversible one. From the relationship between the current value at  $E_{\text{pc}}$  ( $i_{\text{pc}}$ ) and  $\nu^{1/2}$ ,<sup>31</sup> the diffusion coefficient ( $D_{\text{O}}$ ) of  $\text{UO}_2(\text{gha})\text{DMSO}$  in this system was estimated as  $2.8 \times 10^{-7}\text{ cm}^2\cdot\text{s}^{-1}$  at  $298\text{ K}$ .

To determine the electron stoichiometry ( $n$ ) in the reduction of  $\text{UO}_2(\text{gha})\text{DMSO}$  (Figure 1), a UV-vis spectroelectrochemical experiment was performed. The absorption spectra of the  $\text{DMSO}$  solution dissolving  $\text{UO}_2(\text{gha})\text{DMSO}$  ( $4.0 \times 10^{-4}\text{ M}$ ) and  $0.1\text{ M}$   $\text{TBAPF}_6$  were recorded at different potentials stepwise varied from  $-1.075$  to  $-1.313\text{ V}$  vs  $\text{Fc}/\text{Fc}^+$ . Figure 2

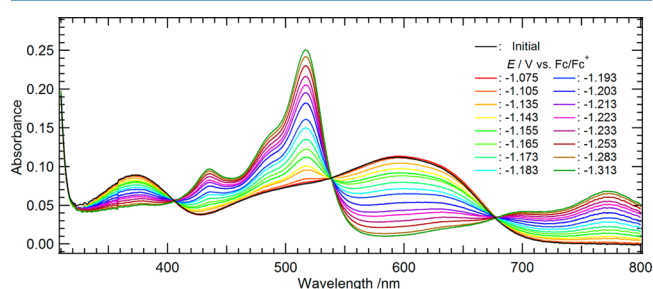


**Figure 2.** UV-vis absorption spectra of  $\text{DMSO}$  solution dissolving  $\text{UO}_2(\text{gha})\text{DMSO}$  ( $4.0 \times 10^{-4}\text{ M}$ ) and  $\text{TBAPF}_6$  ( $0.1\text{ M}$ ) recorded at different potentials from  $-1.075$  to  $-1.313\text{ V}$  vs  $\text{Fc}/\text{Fc}^+$  together with that measured prior to the potential application.

displays the obtained spectra together with that of the initial solution prior to starting this experiment. As the potential on the working electrode is negatively polarized, absorbance increases at around  $370$ ,  $440$ ,  $520$ , and  $770\text{ nm}$ , while that decreases at around  $580\text{ nm}$ . Isosbestic points were observed at  $406$ ,  $538$ , and  $678\text{ nm}$ , indicating that only the redox equilibrium of  $\text{UO}_2(\text{gha})\text{DMSO}$  takes place in this system. Using absorbance at  $517\text{ nm}$ , the concentration ratio ( $C_{\text{O}}/C_{\text{R}}$ ) of the oxidant (i.e.,  $\text{UO}_2(\text{gha})\text{DMSO}$ ) to the reductant at each potential was calculated. The relationship between  $C_{\text{O}}/C_{\text{R}}$  and  $E$  should follow the Nernstian equation, eq 1.

$$E = E^{\circ'} + (RT/nF)\ln(C_{\text{O}}/C_{\text{R}}) \quad (1)$$

where  $E^{\circ'}$ ,  $R$ ,  $T$ , and  $F$  are the formal potential of the redox reaction of interest, the gas constant ( $8.314\text{ J}\cdot\text{mol}^{-1}\cdot\text{K}^{-1}$ ), the absolute temperature (here  $298\text{ K}$ ), and the Faraday constant ( $96485\text{ C}\cdot\text{mol}^{-1}$ ), respectively. In the  $\ln(C_{\text{O}}/C_{\text{R}})-E$  plot (Figure S2, Supporting Information), the slope and intercept of the best fit line of eq 1 to the data points are  $0.028$  and  $-1.195$ , respectively. Consequently, the electron stoichiometry  $n$  has been evaluated as  $0.92$ , which reveals that  $\text{UO}_2(\text{gha})\text{DMSO}$  undergoes the following one-electron reduction in this system.



The intercept ( $-1.195\text{ V}$  vs  $\text{Fc}/\text{Fc}^+$ ) corresponds to  $E^{\circ'}$  of the  $[\text{UO}_2(\text{gha})\text{DMSO}]^-/\text{UO}_2(\text{gha})\text{DMSO}$  redox couple, which is in agreement with that observed in the CV experiments.



The lowest  $E$ ,  $-1.313$  V vs  $\text{Fc}/\text{Fc}^+$ , is lower than  $E^{\circ}$  by  $0.118$  V, which is enough negative to give 99% mole fraction of the reductant in accordance with eq 1. Therefore, the absorption spectrum recorded at this potential is assigned to that of  $[\text{UO}_2(\text{gha})\text{DMSO}]^-$  in DMSO. The molar absorption spectra of  $\text{UO}_2(\text{gha})\text{DMSO}$  and  $[\text{UO}_2(\text{gha})\text{DMSO}]^-$  in DMSO are compared in Figure 3. In our former investigations,<sup>6,7</sup> it has

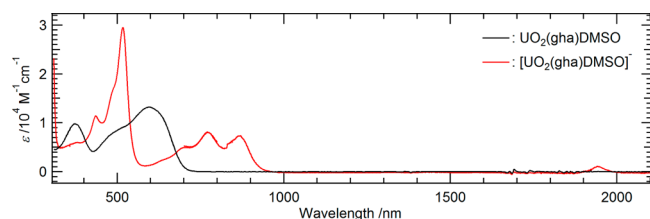


**Figure 3.** Molar absorption spectra of  $\text{UO}_2(\text{gha})\text{DMSO}$  (black) and  $[\text{UO}_2(\text{gha})\text{DMSO}]^-$  (red) in DMSO. Noises at 1700–1900 nm arise from the solvent.

been clarified that the electrochemical reduction of a uranyl(VI) complex usually affords the corresponding uranyl(V) species. Although the formed uranyl(V) always suffers from its decomposition governed by oxidation and disproportionation ( $2\text{U(V)} \rightarrow \text{U(IV)} + \text{U(VI)}$ ), a uranyl(V) complex stabilized by strong auxiliary ligands generally exhibits characteristic absorption bands at 650, 750, 900, 1450, and 1900 nm arising from electric-dipole forbidden  $f-f$  transition in  $5f^1$  configuration and charge transfer from the axial oxygen atoms to  $\text{U}^{5+}$ .<sup>7b,c,32</sup> In contrast, the absorption spectrum of  $[\text{UO}_2(\text{gha})\text{DMSO}]^-$  in the current system (Figure 3) is clearly different from those of the uranyl(V) complexes reported so far.<sup>7b,c</sup> There are two peaks and one shoulder at 870, 770, and 700 nm with significantly larger molar absorptivities ( $\epsilon$ , 5000–8100  $\text{M}^{-1}\cdot\text{cm}^{-1}$ ), while no specific bands and shoulders are lying in the range from 900 to 1900 nm. If  $\text{U}^{5+}$  occurs in  $[\text{UO}_2(\text{gha})\text{DMSO}]^-$ , another characteristic peak should be observed at 1400–1600 nm. Although an additional absorption band has been actually observed at 1940 nm ( $\epsilon = 1100 \text{ M}^{-1}\cdot\text{cm}^{-1}$ ), it is difficult to find the similarity of the absorption spectrum of  $[\text{UO}_2(\text{gha})\text{DMSO}]^-$  with those of the other uranyl(V) complexes. Therefore, the formal oxidation state of U in  $[\text{UO}_2(\text{gha})\text{DMSO}]^-$  is unlikely to be +5 despite the one-electron reduction of  $\text{UO}_2(\text{gha})\text{DMSO}$ . Our next interest is which part of  $\text{UO}_2(\text{gha})\text{DMSO}$  is reduced through the electrochemical reaction affording  $[\text{UO}_2(\text{gha})\text{DMSO}]^-$ . However, it is not a straightforward task to experimentally identify the location of the unpaired electron in the reductant. Therefore, we decided to have support from the quantum chemical calculations.

### 3.2. DFT Calculations for $\text{UO}_2(\text{gha})\text{DMSO}$ and $[\text{UO}_2(\text{gha})\text{DMSO}]^-$ and Related Uranyl(V/VI) Complexes.

**3.2.1.  $\text{UO}_2(\text{gha})\text{DMSO}$  and  $[\text{UO}_2(\text{gha})\text{DMSO}]^-$ .** First, the structure optimization of  $\text{UO}_2(\text{gha})\text{DMSO}$  was performed. The optimized structure is shown in Figure 4. The selected bond distances are summarized in Table 1 together with those of crystalline  $\text{UO}_2(\text{gha})\text{OH}_2$ <sup>29a</sup> and  $[\text{UO}_2(\text{gha})]_2$  (Figure S1, Supporting Information). Full metrics in these complexes are compared in Figure S3 (Supporting Information). As a result, the bond distances in the optimized structure are in good agreement with those of the experimental data within  $0.02$  Å for all U–O distances except for U– $\text{O}_{\text{solv}}$ . The difference in U– $\text{O}_{\text{solv}}$  (ca.  $0.03$  Å) is not very surprising, because the different

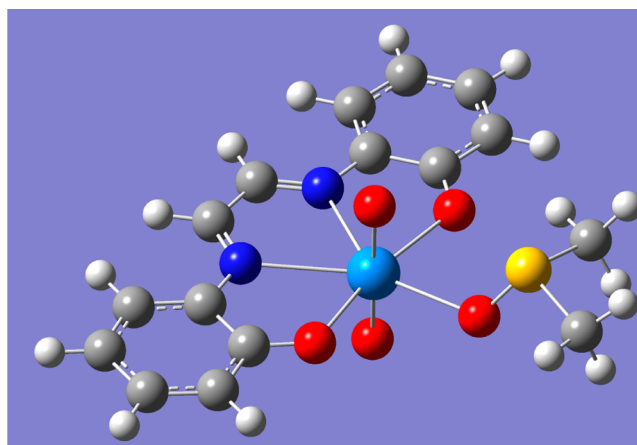


**Figure 4.** Optimized structure of  $\text{UO}_2(\text{gha})\text{DMSO}$ . Light blue, U; yellow, S; red, O; blue, N; gray, C; white, H.

**Table 1.** Selected Bond Distances (R/Å) in Optimized Structures of  $\text{UO}_2(\text{gha})\text{DMSO}$  and  $[\text{UO}_2(\text{gha})\text{DMSO}]^-$  Together with Those of  $\text{UO}_2(\text{gha})\text{OH}_2$  and  $[\text{UO}_2(\text{gha})]_2$  in Crystalline States

	$\text{UO}_2(\text{gha})\text{OH}_2^a$	$[\text{UO}_2(\text{gha})]_2^b$	$\text{UO}_2(\text{gha})\text{DMSO}$	$[\text{UO}_2(\text{gha})\text{DMSO}]^-$	$\Delta R$ (mean)
U– $\text{O}_{\text{ax}}$	1.77	1.762(5)	1.784	1.790	+0.015
	1.77	1.758(5)	1.779	1.802	
U– $\text{O}_{\text{eq}}$	2.33	2.253(5)	2.295	2.293	–0.002
	2.36	2.443(5) <sup>c</sup>	2.345	2.344	
U– $\text{O}_{\text{solv}}$	2.42	2.425(5) <sup>c</sup>	2.446	2.545	+0.099
U–N	2.54	2.567(6)	2.604	2.536	–0.070
	2.56	2.539(6)	2.609	2.537	
N– $\text{C}_{20,21}$	1.28	1.282(9)	1.302	1.340	+0.038
	1.31	1.300(9)	1.303	1.341	
$\text{C}_{20}^-$ / $\text{C}_{21}$	1.44	1.44(1)	1.437	1.396	–0.041

<sup>a</sup>X-ray crystallographically determined by Bandoli et al.<sup>29a</sup> <sup>b</sup>This work (Figure S1, Supporting Information). <sup>c</sup>Interatomic distances between U and bridging phenolic oxygen atom.

solvent molecules may give different distances. Although the computed U–N distances show larger deviations from the crystal structure by  $0.06$  Å, such a difference should be still acceptable. The same calculations were also performed for the reductant,  $[\text{UO}_2(\text{gha})\text{DMSO}]^-$ , resulting in atomic geometries with no imaginary frequencies (Figure S4, Supporting Information) which are very similar to those of the oxidant.

The optimized structure of  $[\text{UO}_2(\text{gha})\text{DMSO}]^-$  should also be compared with the actual one experimentally evidenced. However, our attempts to crystallize this species (e.g., vapor diffusion of ether) were unsuccessful to date. The important

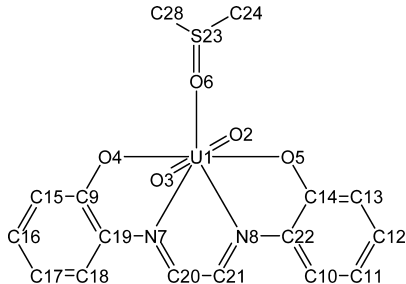
point would be choice of a counteranion. Formerly, potassium ion embedded in a crown ether was employed to crystallize the reduced uranyl complexes with  $-1$  charge by other research group.<sup>10</sup> In these cases, the axial oxygen atom of the uranyl moiety also makes a coordination bond with  $K^+$ . This effect is, however, unfavorable, because it will complicate comparison and interpretation of the calculated structures present alone. The other choice is the quaternary ammonium ion, which has already been introduced in the current system as a supporting electrolyte. However, it is not simple to recover the millimolar reductant from the submolar electrolyte matrix in little volatile DMSO (bp 189 °C). The structural information on  $[UO_2(gha)DMSO]^-$  in DMSO could be in situ obtained by X-ray absorption spectroscopy as we have done formerly.<sup>7e</sup>

The variation in the interatomic distances ( $\Delta R$ ) of  $UO_2(gha)DMSO$  and  $[UO_2(gha)DMSO]^-$  through the reduction is relatively significant in U–N ( $-0.07$  Å) and U–O<sub>solv</sub> ( $+0.10$  Å), while those of U–O<sub>eq</sub> ( $0.00$  Å) and U=O<sub>ax</sub> ( $+0.01$  Å) are very small or virtually negligible. In former studies, it was clarified that the U=O<sub>ax</sub> distances are lengthened about  $0.05$ – $0.10$  Å by reducing  $U^{6+}$  to  $U^{5+}$ ,<sup>7e,33</sup> whereas the atomic geometries of multidentate ligand(s) in the equatorial plane are not affected greatly. Therefore, the current computed structures of  $UO_2(gha)DMSO$  and  $[UO_2(gha)DMSO]^-$  suggest that the unpaired electron in  $[UO_2(gha)DMSO]^-$  would not localize at U, but somewhere on the ligands in the equatorial plane.

The frequency calculation results also lead us to the same conclusion. It is well-known that the uranyl ion has a linear O=U=O geometry which shows characteristic symmetric ( $\nu_1$ ) and asymmetric ( $\nu_3$ ) stretching vibrations in Raman and IR spectra, respectively. In the previous studies, large red shifts of the  $\nu_1$  and  $\nu_3$  frequencies ( $\Delta\nu_1 \approx -60$   $cm^{-1}$ ,  $\Delta\nu_3 \approx -130$   $cm^{-1}$ ) were observed in the reduction from  $U^{6+}$  to  $U^{5+}$ .<sup>7a,d,34</sup> Additionally, the Schiff base compounds usually exhibit a strong IR absorption arising from C=N stretching ( $\nu_{C=N}$ ) in the azomethine groups ( $-N=CH-$ ) at  $1500$ – $1650$   $cm^{-1}$ , which is not largely affected by the difference in the oxidation state of U. In our DFT calculations, the  $\nu_1$  and  $\nu_3$  frequencies of  $[UO_2(gha)DMSO]^-$  are  $845.19$  and  $928.40$   $cm^{-1}$ , respectively. These values are smaller than those in  $UO_2(gha)DMSO$  ( $\nu_1$ ,  $872.33$   $cm^{-1}$ ;  $\nu_3$ ,  $959.72$   $cm^{-1}$ ), but the differences are only  $27$  and  $30$   $cm^{-1}$  for  $\nu_1$  and  $\nu_3$ , respectively, which are not suggestive of difference in the oxidation state of U in these complexes. The  $\nu_3$  frequency was experimentally observed at  $950$   $cm^{-1}$  in the IR spectrum, demonstrating the validity of the frequency calculation. In summary, these results suggest that the oxidation state of U seems not to be largely affected by the reduction from  $UO_2(gha)DMSO$  to  $[UO_2(gha)DMSO]^-$ . The calculated frequencies of  $\nu_{C=N}$  and S=O stretching in the coordinated DMSO ( $\nu_{S=O}$ ) in the oxidant are  $1639.59$  and  $1026.18$   $cm^{-1}$ , respectively, whereas similar values have also been obtained in the reductant ( $\nu_{C=N}$ ,  $1615.92$   $cm^{-1}$ ;  $\nu_{S=O}$ ,  $1035.26$   $cm^{-1}$ ).

For further discussion about location of the unpaired electron in  $[UO_2(gha)DMSO]^-$ , the calculated spin density distribution is summarized in Table 2. As a result, it was clarified that the total fraction of the spin density in the  $-N(7)=C(20)-C(21)=N(8)-$  moiety is  $0.735$ . Most of the remaining fractions are dispersed into the C atoms of the phenyl groups. In contrast, the spin density on U is close to zero. Consequently, the unpaired electron which gives the electronic spin  $S = 1/2$  is mainly localized on the  $-N=C-C=$

**Table 2.** Calculated Spin Densities on Non-Hydrogen Atoms of  $[UO_2(gha)DMSO]^-$  Together with Atomic Notations



atom	spin density	atom	spin density	atom	spin density
U1	-0.0141	C10	0.1088	C18	0.1079
O2	0.0087	C11	-0.0391	C19	-0.0708
O3	0.0087	C12	0.0931	C20	0.1260
O4	0.0145	C13	-0.0169	C21	0.1122
O5	0.0164	C14	0.0600	C22	-0.0729
O6	0.0000	C15	-0.0176	S23	0.0004
N7	0.2438	C16	0.0924	C24	0.0000
N8	0.2528	C17	-0.0406	C28	0.0001
C9	0.0578				

N- moiety in  $[UO_2(gha)DMSO]^-$ . Therefore, the formal oxidation state of U remains unchanged at  $+6$  even after the reduction. This conclusion is corroborated by very similar natural charges<sup>35</sup> on U in the different redox states, which have been estimated as  $1.439$  for  $UO_2(gha)DMSO$  and  $1.411$  for  $[UO_2(gha)DMSO]^-$ .

Molecular orbital (MO) distribution also provides us helpful information to visualize where the unpaired electron is present in the molecule of interest. In a usual one-electron reduction reaction, the electron should be injected into the lowest unoccupied MO (LUMO) of a molecule with a closed electronic configuration. This MO is no longer LUMO in the reductant, but gets to be called the singly occupied MO (SOMO). Therefore, our DFT calculation results should be examined about the distributions of LUMO of the oxidant and SOMO of the reductant which are depicted in Figures 5 and S5 (Supporting Information), respectively. It can be found that the two MOs are almost identical to each other in their spatial distribution. It should be emphasized that the contributions of atomic orbitals (AOs) of U are very small ( $2.4\%$  in the oxidant,

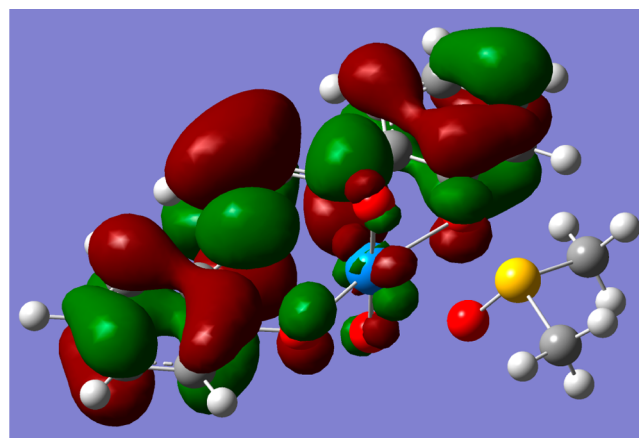


**Figure 5.** Distribution of lowest unoccupied molecular orbital in  $UO_2(gha)DMSO$ . The isovalue of the surface is  $0.02$  au.

1.8% in the reductant) in both cases, while those of AOs in atoms constructing the  $\text{gha}^{2-/3-}$  ligand are exclusively predominant. These MOs should have a character of a  $\pi^*$  orbital of the ligand. Therefore, there is little chance for the unpaired electron to stay in U.

In conclusion, all the findings from the experimental UV–vis–NIR absorption spectroscopy and the theoretical DFT calculations indicate that the formal oxidation state of U remains unchanged at +6 even in the reduction from  $\text{UO}_2(\text{gha})\text{DMSO}$  to  $[\text{UO}_2(\text{gha})\text{DMSO}]^-$ . In addition, the DFT calculations gave a suggestion that the unpaired electron in  $[\text{UO}_2(\text{gha})\text{DMSO}]^-$  is mainly located at  $-\text{N}=\text{C}-\text{C}=\text{N}-$  moiety of the Schiff base ligand. This means that the character of  $\text{gha}^{2-}$  is redox *noninnocent* in this system. Another ligand in the equatorial plane, DMSO, seems to be *innocent* from all the viewpoints in the DFT calculations.

**3.2.2. Related Uranyl(V/VI) Complexes.** At this stage, we wondered if the formal oxidation states of U in the uranyl(V) complexes we reported earlier are truly +5. Therefore, we performed DFT calculations for the uranyl(VI) complexes  $[\text{UO}_2(\text{salophen})\text{DMSO}]$ ,  $[\text{UO}_2(\text{dbm})_2\text{DMSO}]$ , and  $[\text{UO}_2(\text{saldien})]$ ; see Chart 1, all of which were experimentally suggested to give the corresponding uranyl(V) species.

The structure optimization for each uranyl(VI) complex was performed, followed by frequency calculation. The optimized structures of these uranyl(VI) complexes are shown in Figure S6 (Supporting Information), and the selected bond distances and frequencies are summarized in Tables S2–4 (Supporting Information) together with those obtained experimentally. The calculated bond distances agree with those from X-ray crystallography within 0.06, 0.05, and 0.10 Å for  $[\text{UO}_2(\text{salophen})\text{DMSO}]$ ,  $[\text{UO}_2(\text{dbm})_2\text{DMSO}]$ , and  $[\text{UO}_2(\text{saldien})]$ , respectively. The calculated  $\nu_3$  frequency of each complex is also in good agreement with that experimentally observed by taking the scaling factor 0.95 into account. These results on each uranyl(VI) species suggest that its optimized structure was successfully obtained. In all the complexes, disagreements of the U–N distances ( $\Delta R = 0.05\text{--}0.10$  Å) tend to be somewhat larger than those of U–O<sub>eq</sub> ( $\Delta R = 0.00\text{--}0.08$  Å). However, no improvements were observed even in the use of larger basis sets like 6-311G(d,p) for nonmetallic elements.

The main concern on this section is the shapes of LUMOs in  $[\text{UO}_2(\text{salophen})\text{DMSO}]$ ,  $[\text{UO}_2(\text{dbm})_2\text{DMSO}]$ , and  $[\text{UO}_2(\text{saldien})]$ . The LUMOs of these complexes were drawn on their molecular structures in Figure 6. Although some contributions from the auxiliary ligands ( $\text{salophen}^{2-}$ ,  $\text{dbm}^-$ ,  $\text{saldien}^{2-}$ ) to LUMOs can be found, the main component in each system is obviously a  $5f\delta_u$  orbital of U. Therefore, the additional electron in the reduction of these uranyl(VI) complexes would be inserted in U 5f orbitals shown in Figure 6, i.e., the reduction product is uranyl(V).

We have also tried the calculations for structure optimization and frequency analyses of the uranyl(V) complexes,  $[\text{UO}_2(\text{salophen})\text{DMSO}]^-$ ,  $[\text{UO}_2(\text{dbm})_2\text{DMSO}]^-$ , and  $[\text{UO}_2(\text{saldien})]^-$ . Although the shapes of SOMOs of these uranyl(V) complexes (Figure S7, Supporting Information) are somewhat different from LUMOs of the corresponding uranyl(VI) in Figure 6, the main contributor to SOMO in each uranyl(V) complex is undoubtedly U  $5f\delta_u$  orbital in a similar manner to LUMOs of uranyl(VI). Furthermore, the calculated spin densities in U of  $[\text{UO}_2(\text{salophen})\text{DMSO}]^-$ ,  $[\text{UO}_2(\text{dbm})_2\text{DMSO}]^-$ , and  $[\text{UO}_2(\text{saldien})]^-$  were 1.077, 0.967, and 1.034, respectively. Consequently, the DFT

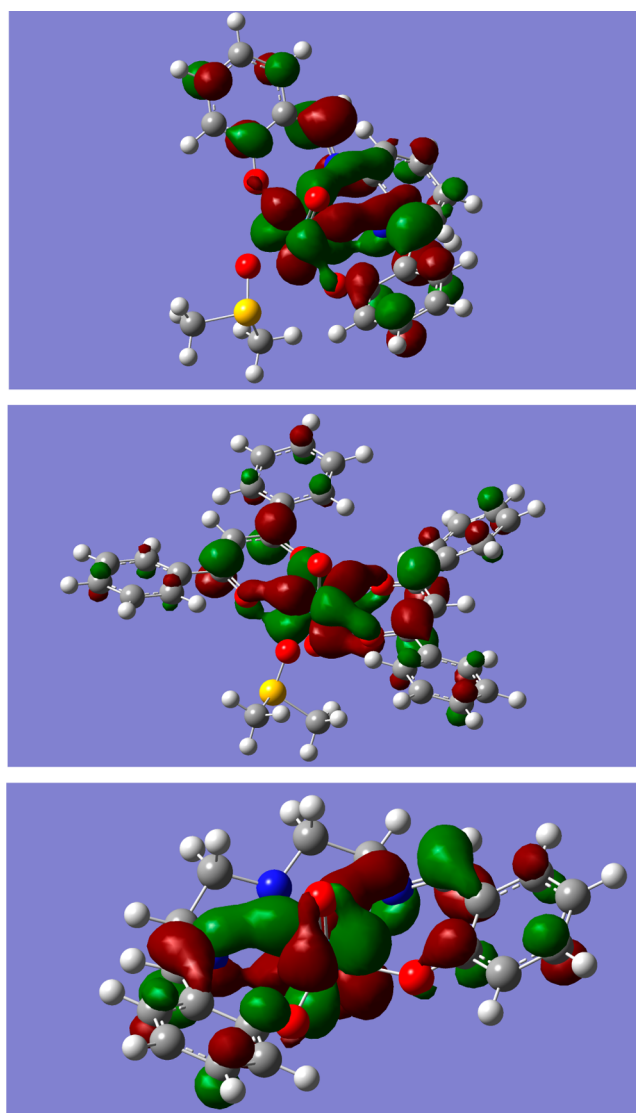


**Figure 6.** Distribution of lowest unoccupied molecular orbitals in  $[\text{UO}_2(\text{salophen})\text{DMSO}]$  (top),  $[\text{UO}_2(\text{dbm})_2\text{DMSO}]$  (middle), and  $[\text{UO}_2(\text{saldien})]$  (bottom). The isovalue of the surface is 0.02 au.

calculations for  $[\text{UO}_2(\text{salophen})\text{DMSO}]^-/[\text{UO}_2(\text{salophen})\text{DMSO}]$ ,  $[\text{UO}_2(\text{dbm})_2\text{DMSO}]^-/[\text{UO}_2(\text{dbm})_2\text{DMSO}]$ , and  $[\text{UO}_2(\text{saldien})]^-/[\text{UO}_2(\text{saldien})]$  revealed that  $\text{salophen}^{2-}$ ,  $\text{dbm}^-$ ,  $\text{saldien}^{2-}$ , and DMSO in these systems are *innocent*, and that the formal oxidation states of U in their reductants are certainly +5. Therefore, these reductants show the characteristic properties of uranyl(V) different from  $[\text{UO}_2(\text{gha})\text{DMSO}]^-$ .

The optimized structures of  $[\text{UO}_2(\text{salophen})\text{DMSO}]^-$ ,  $[\text{UO}_2(\text{dbm})_2\text{DMSO}]^-$ , and  $[\text{UO}_2(\text{saldien})]^-$  are actually not always in harmony with those found in our former EXAFS experiments<sup>7e,29b</sup> as shown in Tables S2–S4 (Supporting Information). In the current DFT calculations, no solvent effects were taken into account, while the EXAFS data were obtained from the solution samples. This difference might be responsible for the disagreement found in the atomic coordinates and the interatomic distances.<sup>10f,36</sup> The bonding interaction between U and the donor atoms in the equatorial plane may be affected by the solvation more largely than those of U–O<sub>ax</sub> because the former is actually weaker than the latter. As a matter of fact, the deviation in the interatomic distance is



much more remarkable in the equatorial plane of  $[\text{UO}_2]^+$  compared with the axial direction. Nevertheless, we find systematic trends in the structure modification upon reduction from U(VI) to U(V). For instance, the  $\nu_1$  and  $\nu_3$  frequencies were predicted to decrease with the reduction in all the systems. Such a phenomenon was experimentally demonstrated by the vibrational spectroscopy.<sup>7a,d</sup> Another general tendency found in these structures is lengthening of the U–O<sub>ax</sub> bond by 0.04–0.05 Å, being in line with the experimental evidence obtained by EXAFS and X-ray crystallography.<sup>5,7e,9a,b,10d,f</sup>

It should be interesting to examine why  $\text{gha}^{2-}$  in  $\text{UO}_2(\text{gha})\text{-DMSO}$  is *noninnocent* and why the others studied here are *innocent*. The difference in energy levels of LUMOs may give a hint to answer to these questions. Figure 7 shows the energy

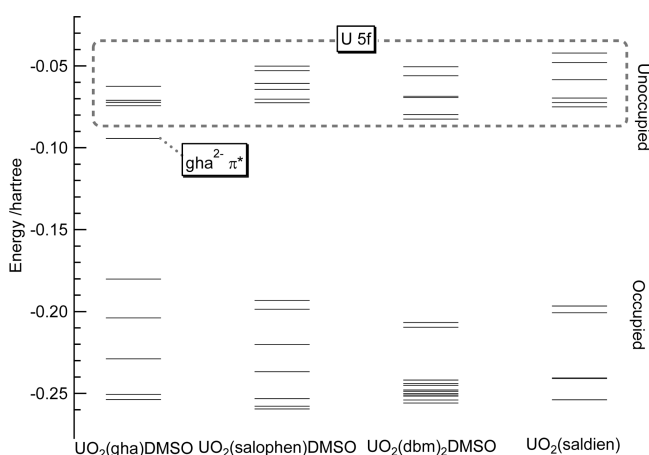


**Figure 7.** Calculated MO energy diagrams of uranyl(VI) complexes.

diagrams of MOs in the uranyl(VI) complexes extracted from the DFT calculation results. In  $\text{UO}_2(\text{salophen})\text{DMSO}$ ,  $\text{UO}_2(\text{dbm})_2\text{DMSO}$ , and  $\text{UO}_2(\text{saldien})$ , MOs predominantly consisting of the U 5f orbitals are lying among the LUMOs. Although such a tendency is also observed in  $\text{UO}_2(\text{gha})\text{DMSO}$ , another unoccupied MO is present at the lower position in energy than U 5f orbitals. This MO has already been shown in Figure 5. The  $\pi^*$  character of LUMO in  $\text{UO}_2(\text{gha})\text{DMSO}$  was evidenced by its close similarity with that of  $\text{gha}^{2-}$  (Figure S8, Supporting Information), which resulted from the single point energy calculation of  $\text{gha}^{2-}$  under the same computation level, basis sets, and atomic geometries as  $\text{UO}_2(\text{gha})\text{DMSO}$  except for removal of  $[\text{UO}_2]^{2+}$  and DMSO. Actually, LUMO+1 in  $\text{UO}_2(\text{gha})\text{DMSO}$  consists almost purely of U  $5f_{\delta_a}$  orbital as shown in Figure S9 (Supporting Information). The narrower HOMO–LUMO gap can be related to the higher  $E^{\circ}$  of  $[\text{UO}_2(\text{gha})\text{DMSO}]^-/\text{UO}_2(\text{gha})\text{DMSO}$  ( $-1.195$  V vs  $\text{Fc}/\text{Fc}^+$ ) than those of other redox couples studied here ( $E^{\circ} = -1.550$  V for  $[\text{UO}_2(\text{salophen})\text{DMSO}]^-/\text{UO}_2(\text{salophen})\text{DMSO}$ ,  $-1.362$  V for  $[\text{UO}_2(\text{dbm})_2\text{DMSO}]^-/\text{UO}_2(\text{dbm})_2\text{DMSO}$ ,  $-1.584$  V for  $[\text{UO}_2(\text{saldien})]^-/\text{UO}_2(\text{saldien})$ ).<sup>6,7b,c</sup> The characteristic contribution of the  $\pi^*$  orbital in  $\text{UO}_2(\text{gha})\text{DMSO}$  can also be confirmed experimentally. The solid  $\text{UO}_2(\text{gha})\text{DMSO}$  and its DMSO solution are significantly colored in purple, while the others are yellow or orange. As a matter of fact,  $\text{UO}_2(\text{gha})\text{-DMSO}$  exhibits the unique absorption band and shoulders at 500–600 nm as shown in Figure 2. The TD DFT calculation excellently reproduces the experimental UV–vis absorption spectrum and provides the assignment for each electronic transition (Figure S10, Supporting Information). The largest

contribution to the absorption band lowest in energy is attributable to the HOMO–LUMO transition which significantly has a character of  $\pi-\pi^*$  in  $\text{gha}^{2-}$ . Such a transition is never found in the other uranyl(VI) complexes studied here, because there are no  $\pi^*$  orbitals lying under the U 5f orbitals. In conclusion, the *innocence* of ligand(s) in the uranyl complexes is determined by the energy level of LUMO in the ligand compared with those of U 5f orbitals.

#### 4. CONCLUSION

In this paper, we studied the detailed redox chemistry of  $\text{UO}_2(\text{gha})\text{DMSO}$  by means of electro- and spectroelectrochemical techniques. Our initial motivation was only to find a new uranyl(V) complex using  $\text{gha}^{2-}$  ligand to expand the coordination chemistry of this unstable and exotic oxidation state, whereas it was also known that  $\text{gha}^{2-}$  bridging two Ru centers could show the *noninnocent* behavior.<sup>37</sup> The one-electron reduction of the parent  $\text{UO}_2(\text{gha})\text{DMSO}$  in the DMSO solution was experimentally evidenced, while the observed characteristics in the absorption spectrum of the generated  $[\text{UO}_2(\text{gha})\text{DMSO}]^-$  turned out to be much different from those of uranyl(V) species known so far. Therefore, we had doubt whether the oxidation state of U in  $[\text{UO}_2(\text{gha})\text{-DMSO}]^-$  is certainly +5 or not. This argument was reasonably concluded by the DFT calculations. The unpaired electron in  $[\text{UO}_2(\text{gha})\text{DMSO}]^-$  was found to be exclusively localized on the tetradentate Schiff base ligand, namely,  $\text{gha}^{\bullet 3-}$  anion radical. In contrast, there was no evidence to suggest the reduction of uranium, demonstrating that its oxidation state does not change from +6 regardless of the redox reaction between  $\text{UO}_2(\text{gha})\text{-DMSO}$  and  $[\text{UO}_2(\text{gha})\text{DMSO}]^-$ . In other uranyl(V/VI) couples we reported previously, the situation is much different. The unpaired electron is exclusively localized on U atoms in  $[\text{UO}_2(\text{salophen})\text{DMSO}]^-$ ,  $[\text{UO}_2(\text{dbm})_2\text{DMSO}]^-$ , and  $[\text{UO}_2(\text{saldien})]^-$ , suggesting that the formal oxidation state of U in these complexes is +5. This is in line with their common characteristics of the absorption spectra. The disagreement in the optical properties of  $[\text{UO}_2(\text{gha})\text{DMSO}]^-$  with uranyl(V) complexes is fully addressed in terms of difference in the redox *innocence* of the equatorial auxiliary ligand(s). To the best of our knowledge,  $[\text{UO}_2(\text{gha})\text{DMSO}]^-/\text{UO}_2(\text{gha})\text{DMSO}$  currently studied is the first example of the redox *noninnocent* ligand system in the coordination chemistry of uranyl(VI). In recent research activities, some actinide complexes are frequently subjected to catalysis of organic syntheses. However, such use is extensively limited to low-valent organoactinides, which are always very unstable under ambient condition and, therefore, must be handled with great care and proficiency. In contrast, uranyl(VI) is most accessible in the various oxidation states of uranium, which is also most available in the actinide elements. If some catalytic activity arising from the *noninnocent* ligand system of uranyl(VI) is established, it may lead to one of efficient and sophisticated use of natural and depleted uranium resources.

#### ■ ASSOCIATED CONTENT

##### Supporting Information

ORTEP drawing of  $[\text{UO}_2(\text{gha})]_2$ , Nernstian plot for Figure 2, full metrics in uranyl–gha complexes, optimized structures and MO distributions of uranyl(V/VI) complexes and  $\text{gha}^{2-}$ , molar absorption spectrum of  $\text{UO}_2(\text{gha})\text{DMSO}$  in DMSO together with absorption peak positions predicted by TD DFT calculation, electrochemical data of  $\text{UO}_2(\text{gha})\text{DMSO}$  in Figure

l, and experimental and calculated selected bond distances and characteristic frequencies of uranyl(V/VI) complexes. CIF file for  $\text{UO}_2(\text{gha})\text{DMSO}$ . This material is available free of charge via the Internet at <http://pubs.acs.org>.

## AUTHOR INFORMATION

### Corresponding Author

\*E-mail: [ktakao@nr.titech.ac.jp](mailto:ktakao@nr.titech.ac.jp)

### Notes

The authors declare no competing financial interest.

## ACKNOWLEDGMENTS

This work was partly supported by the research grant provided by Seikei University.

## REFERENCES

- (1) Katz, J. J.; Seaborg, G. T. *The Chemistry of the Actinide Elements*, 2nd ed.; Chapman and Hall: London, NY, 1986.
- (2) Benedict, M.; Pigford, T. H.; Levi, H. W. *Nuclear Chemical Engineering*, 2nd ed.; McGraw-Hill: United States, 1981.
- (3) (a) Efurud, D. W.; Runde, W.; Banar, J. C.; Janecky, D. R.; Kaszuba, J. P.; Palmer, P. D.; Roensch, F. R.; Tait, C. D. *Environ. Sci. Technol.* **1998**, *32*, 3893–3900. (b) Clark, D. L.; Hobart, D. E.; Neu, M. P. *Chem. Rev.* **1995**, *95*, 25–48. (c) Denecke, M. *Coord. Chem. Rev.* **2006**, *250*, 730–754. (d) Walther, C.; Denecke, M. A. *Chem. Rev.* **2013**, *113*, 995–1015. (e) Guillaumont, R.; Fanghanel, T.; Neck, V.; Fuger, J.; Palmer, D. A.; Grenthe, I.; Rand, M. H. *Update on the Chemical Thermodynamics of Uranium, Neptunium, Plutonium, Americium and Technetium*; Elsevier B.V.: Amsterdam, The Netherlands, 2003.
- (4) (a) Heal, H. G. *Trans. Faraday Soc.* **1949**, *45*, 1–11. (b) Heal, H. G.; Thomas, J. G. N. *Trans. Faraday Soc.* **1949**, *45*, 11–20. (c) Newton, T. W.; Baker, F. B. *Inorg. Chem.* **1965**, *4*, 1166–1170. (d) Ekstrom, A. *Inorg. Chem.* **1974**, *13*, 2237–2241. (e) McDuffie, B.; Reilley, C. N. *Anal. Chem.* **1966**, *38*, 1881–1887. (f) Kern, D. M. H.; Orlemann, E. F. *J. Am. Chem. Soc.* **1949**, *71*, 2102–2106.
- (5) Berthet, J. C.; Nierlich, M.; Ephritikhine, M. *Angew. Chem., Int. Ed.* **2003**, *42*, 1952–1954.
- (6) Mizuoka, K.; Kim, S. Y.; Hasegawa, M.; Hoshi, T.; Uchiyama, G.; Ikeda, Y. *Inorg. Chem.* **2003**, *42*, 1031–1038.
- (7) (a) Mizuoka, K.; Ikeda, Y. *Radiochim. Acta* **2004**, *92*, 631–635. (b) Takao, K.; Kato, M.; Takao, S.; Nagasawa, A.; Bernhard, G.; Hennig, C.; Ikeda, Y. *Inorg. Chem.* **2010**, *49*, 2349–2359. (c) Mizuoka, K.; Tsushima, S.; Hasegawa, M.; Hoshi, T.; Ikeda, Y. *Inorg. Chem.* **2005**, *44*, 6211–6218. (d) Mizuoka, K.; Ikeda, Y. *Inorg. Chem.* **2003**, *42*, 3396–3398. (e) Takao, K.; Tsushima, S.; Takao, S.; Scheinost, A. C.; Bernhard, G.; Ikeda, Y.; Hennig, C. *Inorg. Chem.* **2009**, *48*, 9602–9604. (f) Ogura, T.; Takao, K.; Sasaki, K.; Arai, T.; Ikeda, Y. *Inorg. Chem.* **2011**, *50*, 10525–10527.
- (8) (a) Berthet, J. C.; Siffredi, G.; Thuery, P.; Ephritikhine, M. *Chem. Commun.* **2006**, 3184–3186. (b) Berthet, J. C.; Siffredi, G.; Thuery, P.; Ephritikhine, M. *Dalton Trans.* **2009**, 3478–3494.
- (9) (a) Hayton, T. W.; Wu, G. *J. Am. Chem. Soc.* **2008**, *130*, 2005–2014. (b) Hayton, T. W.; Wu, G. *Inorg. Chem.* **2008**, *47*, 7415–7423. (c) Hayton, T. W.; Wu, G. *Inorg. Chem.* **2009**, *48*, 3065–3072. (d) Schnaars, D. D.; Wu, G.; Hayton, T. W. *J. Am. Chem. Soc.* **2009**, *131*, 17532–17533. (e) Schettini, M. F.; Wu, G.; Hayton, T. W. *Inorg. Chem.* **2009**, *48*, 11799–11808.
- (10) (a) Burdet, F.; Pecaut, J.; Mazzanti, M. *J. Am. Chem. Soc.* **2006**, *128*, 16512–16513. (b) Natrajan, L.; Burdet, F.; Pecaut, J.; Mazzanti, M. *J. Am. Chem. Soc.* **2006**, *128*, 7152–7153. (c) Nocton, G.; Horeglad, P.; Pecaut, J.; Mazzanti, M. *J. Am. Chem. Soc.* **2008**, *130*, 16633–16645. (d) Horeglad, P.; Nocton, G.; Filinchuk, Y.; Pecaut, J.; Mazzanti, M. *Chem. Commun.* **2009**, 1843–1845. (e) Mougél, V.; Horeglad, P.; Nocton, G.; Pecaut, J.; Mazzanti, M. *Angew. Chem., Int. Ed.* **2009**, *48*, 8477–8480. (f) Nocton, G.; Horeglad, P.; Vetere, V.; Pecaut, J.; Dubois, L.; Maldivi, P.; Edelstein, N. M.; Mazzanti, M. *J. Am. Chem. Soc.* **2010**, *132*, 495–508. (g) Mougél, V.; Biswas, B.; Pecaut, J.; Mazzanti, M. *Chem. Commun.* **2010**, *46*, 8648–8650. (h) Mougél, V.; Horeglad, P.; Nocton, G.; Pecaut, J.; Mazzanti, M. *Chem.—Eur. J.* **2010**, *16*, 14365–14377. (i) Mougél, V.; Pecaut, J.; Mazzanti, M. *Chem. Commun.* **2012**, *48*, 868–870.
- (11) (a) Graves, C. R.; Kiplinger, J. L. *Chem. Commun.* **2009**, 3831–3853. (b) Arnold, P. L.; Love, J. B.; Patel, D. *Coord. Chem. Rev.* **2009**, *253*, 1973–1978. (c) Fortier, S.; Hayton, T. W. *Coord. Chem. Rev.* **2010**, *254*, 197–214. (d) Jones, M. B.; Gaunt, A. J. *Chem. Rev.* **2013**, *113*, 1137–1198.
- (12) Jørgensen, C. K. *Coord. Chem. Rev.* **1966**, *1*, 164–178.
- (13) Matsika, S.; Zhang, Z.; Brozell, S. R.; Blaudeau, J. P.; Wang, Q.; Pitzer, R. M. *J. Phys. Chem. A* **2001**, *105*, 3825–3828.
- (14) Chirik, P. J. *Inorg. Chem.* **2011**, *50*, 9737–9740.
- (15) (a) Zanello, P.; Corsini, M. *Coord. Chem. Rev.* **2006**, *250*, 2000–2022. (b) Kaim, W.; Schwederski, B. *Coord. Chem. Rev.* **2010**, *254*, 1580–1588. (c) Lyaskovskyy, V.; de Bruin, B. *ACS Catal.* **2012**, *2*, 270–279.
- (16) (a) Blake, P. C.; Edelstein, N. M.; Hitchcock, P. B.; Kot, W. K.; Lappert, M. F.; Shalimoff, G. V.; Tian, S. *J. Organomet. Chem.* **2001**, *636*, 124–129. (b) Korobkov, I.; Gambarotta, S.; Yap, G. P. *Angew. Chem., Int. Ed.* **2003**, *42*, 814–818. (c) MacDonald, M. R.; Fieser, M. E.; Bates, J. E.; Ziller, J. W.; Furche, F.; Evans, W. J. *J. Am. Chem. Soc.* **2013**, *135*, 13310–13313. (d) Kraft, S. J.; Williams, U. J.; Daly, S. R.; Schelter, E. J.; Kozimor, S. A.; Boland, K. S.; Kikkawa, J. M.; Forrest, W. P.; Christensen, C. N.; Schwarz, D. E.; Fanwick, P. E.; Clark, D. L.; Conradson, S. D.; Bart, S. C. *Inorg. Chem.* **2011**, *50*, 9838–9848. (e) Li Manni, G.; Walensky, J. R.; Kraft, S. J.; Forrest, W. P.; Perez, L. M.; Hall, M. B.; Gagliardi, L.; Bart, S. C. *Inorg. Chem.* **2012**, *51*, 2058–2064.
- (17) (a) Tsushima, S. *J. Phys. Chem. B* **2008**, *112*, 13059–13063. (b) Huang, W.; Xu, W. H.; Su, J.; Schwarz, W. H.; Li, J. *Inorg. Chem.* **2013**, *52*, 14237–14245.
- (18) Bowen, R. P.; Lincoln, S. F.; Williams, E. H. *Inorg. Chem.* **1976**, *15*, 2126–2129.
- (19) Cattalini, L.; Vigato, P. A.; Vidali, M.; Degetto, S.; Casellato, U. *J. Inorg. Nucl. Chem.* **1975**, *37*, 1721–1723.
- (20) Gritzner, G.; Kuta, J. *Pure Appl. Chem.* **1984**, *56* (4), 461–466.
- (21) (a) DeAngelis, T. P.; Heineman, W. R. *J. Chem. Educ.* **1976**, *53*, 594. (b) Heineman, W. R. *J. Chem. Educ.* **1983**, *60*, 305. (c) Endo, A.; Mochida, I.; Shimizu, K.; Satô, G. P. *Anal. Sci.* **1995**, *11*, 457–459.
- (22) Altomare, A.; Casciarano, G.; Giacovazzo, C.; Guagliardi, A. J. *Appl. Crystallogr.* **1993**, *26*, 343–350.
- (23) Sheldrick, G. M. *Acta Crystallogr.* **2008**, *A64*, 112–122.
- (24) *CrystalStructure 4.0*, Crystal Structure Analysis Package; Rigaku Corporation: Tokyo, Japan, 2010.
- (25) Frisch, M. J.; Trucks, G. W.; Schlegel, H. B.; Scuseria, G. E.; Robb, M. A.; Cheeseman, J. R.; Scalmani, G.; Barone, V.; Mennucci, B.; Petersson, G. A.; Nakatsuji, H.; Caricato, M.; Li, X.; Hratchian, H. P.; Izmaylov, A. F.; Bloino, J.; Zheng, G.; Sonnenberg, J. L.; Hada, M.; Ehara, M.; Toyota, K.; Fukuda, R.; Hasegawa, J.; Ishida, M.; Nakajima, T.; Honda, Y.; Kitao, O.; Nakai, H.; Vreven, T.; J. A. Montgomery, J.; Peralta, J. E.; Ogliaro, F.; Bearpark, M.; Heyd, J. J.; Brothers, E.; Kudin, K. N.; Staroverov, V. N.; Keith, T.; Kobayashi, R.; Normand, J.; Raghavachari, K.; Rendell, A.; Burant, J. C.; Iyengar, S. S.; Tomasi, J.; Cossi, M.; Rega, N.; Millam, J. M.; Klene, M.; Knox, J. E.; Cross, J. B.; Bakken, V.; Adamo, C.; Jaramillo, J.; Gomperts, R.; Stratmann, R. E.; Yazyev, O.; Austin, A. J.; Cammi, R.; Pomelli, C.; Ochterski, J. W.; Martin, R. L.; Morokuma, K.; Zakrzewski, V. G.; Voth, G. A.; Salvador, P.; Dannenberg, J. J.; Dapprich, S.; Daniels, A. D.; Farkas, O.; Foresman, J. B.; Ortiz, J. V.; Cioslowski, J.; Fox, D. J. *Gaussian 09, Revision C.01*; Gaussian, Inc.: Wallingford, CT, 2010.
- (26) Lee, C.; Yang, W.; Parr, R. G. *Phys. Rev. B* **1988**, *37*, 785–789.
- (27) Küchle, W.; Dolg, M.; Stoll, H.; Preuss, H. *J. Chem. Phys.* **1994**, *100*, 7535–7542.
- (28) (a) Macak, P.; Tsushima, S.; Wahlgren, U.; Grenthe, I. *Dalton Trans.* **2006**, 3638–3646. (b) Tsushima, S.; Rossberg, A.; Ikeda, A.; Müller, K.; Scheinost, A. C. *Inorg. Chem.* **2007**, *46*, 10819–10826.



(29) (a) Bandoli, G.; Cattalini, L.; Clemente, D. A.; Vidali, M.; Vigato, P. A. *J. Chem. Soc., Chem. Commun.* **1972**, 344. (b) Takao, K.; Ikeda, Y. *Inorg. Chem.* **2007**, *46*, 1550–1562. (c) Takao, K.; Ikeda, Y. *Acta Crystallogr.* **2008**, *E64*, m219–220.

(30) Gottlieb, H. E.; Kotlyar, V.; Nudelman, A. *J. Org. Chem.* **1997**, *62*, 7512–7515.

(31) Heinze, J. *Angew. Chem., Int. Ed. Engl.* **1984**, *23*, 831–847.

(32) (a) Merritt, J. M.; Han, J.; Heaven, M. C. *J. Chem. Phys.* **2008**, *128*, 084304. (b) Tecmer, P.; Govind, N.; Kowalski, K.; de Jong, W. A.; Visscher, L. *J. Chem. Phys.* **2013**, *139*, 034301.

(33) (a) Docrat, T. I.; Mosselmans, J. F. W.; Charnock, J. M.; Whiteley, M. W.; Collison, D.; Livens, F. R.; Jones, C.; Edmiston, M. J. *Inorg. Chem.* **1999**, *38*, 1879–1882. (b) Ikeda, A.; Hennig, C.; Tsushima, S.; Takao, K.; Ikeda, Y.; Scheinost, A. C.; Bernhard, G. *Inorg. Chem.* **2007**, *46*, 4212–4219.

(34) Madic, C.; Hobart, D. E.; Begun, G. M. *Inorg. Chem.* **1983**, *22*, 1494–1503.

(35) Glendening, E. D.; Reed, A. E.; Carpenter, J. E.; Weinhold, F. *NBO Version 3.1*.

(36) Shamov, G. A.; Schreckenbach, G. *J. Phys. Chem. A* **2006**, *110*, 9486–9499.

(37) Kar, S.; Sarkar, B.; Ghuman, S.; Roy, D.; Urbanos, F. A.; Fiedler, J.; Sunoj, R. B.; Jimenez-Aparicio, R.; Kaim, W.; Lahiri, G. K. *Inorg. Chem.* **2005**, *44*, 8715–8722.